Journal of Atomic and Molecular Sciences

ISSN 2075-1303

Global Science Press

Theoretical elaboration about excited state behaviors and fluoride anion sensor mechanism for 2-{[2-(2-Hydroxy-phenyl)-1H-benzoimidazo-5-yl]-phenyl-methylene} malononitrile

Received Jan. 18, 2018,
Accepted Apr. 23, 2018,

DOI: 10.4208/jams.011818.042318a

http://www.global-sci.org/jams/

Jia Li[1], Xiaodong Li[1], Shibo Cheng[2], Peng Song[3], Jinfeng Zhao[3,4,*]

Abstract. In view of the enormous potential of fluorescence chemosensors in recent years, more and more people focus on their developments. In the present work, we theoretically investigate a novel fluorescence sensor 2-{[2-(2-Hydroxy-phenyl)-1H-benzoimidazo-5-yl]-phenyl-methylene}-malononitrile (HBPMM) [*J. Lumin.* ***2016****, 173, 165*] about its excited state intramolecular proton transfer (ESIPT) and probe response mechanism. Based on density functional theory (DFT) and time-dependent density functional theory (TDDFT) methods, we focus on the S_0-state and S_1-state hydrogen bonds dynamical behaviors and confirm that the strengthening intramolecular hydrogen bond in the S_1 state may promote the ESIPT reaction. In view of the photoexcitation, we find that the charge redistribution around hydroxyl moiety plays important roles in providing driving force for ESIPT. And the constructed potential energy curves further verify the ESIPT process of HBPMM should be ultrafast. That is the reason why the normal HBPMM fluorescence cannot be detected in previous experiment. Further, with the addition of fluoride anions, the exothermal deprotonation process occurs spontaneously along with the intermolecular hydrogen bond O-H•••F. It reveals the uniqueness of detecting fluoride anion using HBPMM molecule. As a whole, the fluoride anion inhibits the initial ESIPT process of HBPMM, which results in different fluorescence behaviors. This work presents the clear ESIPT process and fluoride anion sensing mechanism for the novel HBPMM chemosensor.

Keywords: Intramolecular hydrogen bond; Fluoride anion; Charge transfer; ESIPT; MOs.

1. Introduction

In recent years, fluorescence chemosensors have been largely designed and developed due to their tremendous potentials for selective detection about biological and chemical species [1-5]. It is well known that the most important feature of fluorescence sensors should be the changed fluorescence emission in the UV-Vis region, since the observable fluorescence intensities or wavelengths can be affected based on the interactions with surroundings [6-10]. Fluoride anion, a type of essential trace element in human lives, is very important and widely used in industrial process, health, medical, and so on [11-14]. It is also a useful chemical in dental care and treatment of osteoporosis. Although fluoride anions could play important roles in nature, the excessive fluoride ions can result in immune system disruption, environmental pollution, kidney damage, and even cancer [15]. In other words, the detection about fluoride anions should be significant in our life. Given the fluorescence chemosensors have apparent advantages, namely, low cost, high sensitivity, high selectivity, rapid implementation, and so on [16-20], the designing and developing new fluoride ion chemosensors have attracted lots of attention in solution phase in recent years.

Generally, the fluorescence sensors could convert the discrimination of fluoride ions into the fluorescence emission signals. And most of the current fluoride ion chemosensors have been developed via fluoride mediated desilylation of Si-O bond using tert-butyldiphenylsilyl (TBDPS) and tert-butyldimethylsilyl (TBDMS) groups, fluoride anion induced deprotonation via pre-existing intra- or inter- molecular hydrogen bond, and so forth [21-30]. And in the aspect of experiment, the corresponding photophysical and

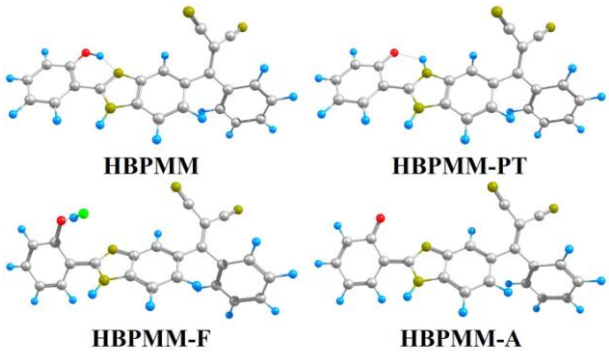

Figure 1: The relative structures of the optimized HBPMM, the proton-transfer HBPPM (HBPPM-PT), the fluoride-anion complex form HBPMM-F, and the anion form HBPMM-A.

[1] *Key Laboratory for Anisotropy and Texture of Materials (Ministry of Education), School of Materials, Northeastern University, Shenyang, Liaoning 110819.*
[2] *Shandong University, Shanda South Road, Jinan, Shandong, China 250100*
[3] *Department of Physics, Liaoning University, Shenyang, Liaoning 110036, China.*
[4] *State Key Laboratory of Molecular Reaction Dynamics, Theoretical and Computational Chemistry, Dalian Institute of Chemical Physics, Chinese Academy of Sciences, Dalian 116023, China.*
Corresponding author: Email: jfzhao1990112@163.com

photochemical characteristics are generally revealed via 1HNMR spectra, time-resolved absorption and emission spectra. And as a kind of complement to experimental techniques, theoretical simulations can be suitable for further exploring the sensor response mechanism.

Recently, a novel fluorescence sensor 2-{[2-(2-Hydroxy-phenyl)-1H-benzoimidazo-5-yl]-phenyl-methylene}-malononitrile (HBPMM) has been designed and synthesized by Gupta and coworkers [31]. Due to the withdrawing -dicyano groups exist in HBPMM molecule, it showed the broad absorption at 370 nm and fluorescence band centered at 505 nm [31]. And the emission spectrum of 505 nm was predicted to be the facilitation of ESIPT phenomenon. While with the addition of fluoride anions, the fluorescence band changes a lot with response the fluoride anion. They suggested that the added fluoride anion may lead to the inhibition of the ESIPT process and the release of initial fluorescence and the anion-form emission [31]. The HBPMM structure has been shown in Figure 1. As far as we know, the theoretical investigations about this type sensors are limited [21-30]. In experiment, just the indirect information about the structural and photochemical properties can be infrared based on experimental manner. Particularly, the mechanism about the uniqueness for detecting fluoride anion cannot be revealed experimentally. It is well known that the chemical reaction mechanism is very important for HBPMM molecule, which can facilitate understanding and controlling the probe response in future. While the quantum chemical calculations about the excited states for HBPMM system might be a reasonable way to clarify the fundamental aspects about its response mechanism for fluoride anion, which can further explain the uniqueness for fluoride anions.

In this present work, therefore, we mainly focus our attention on the excited state dynamical behaviours of HBPMM and its fluoride anion response mechanism. Based on density functional theory (DFT) and time-dependent density functional theory (TDDFT) methods, we verify the validity for fluoride anion response. We deem that the elaborating probe mechanism for HBPM in this work should be useful for design and synthesis novel fluorescent chemosensors in future.

2. Computational Methods

In this work, all the calculations have been performed via Gaussian 09 program suit [32]. As mentioned above, within the framework of DFT and TDDFT methods, the hybrid exchange-correlation functional B3LYP and the triple-ζ valence quality with one set of polarization functions (TZVP) basis set have been selected in all calculations [33-39]. Given the solvent surrounding in previous experiment [31], the tetrahydrofuran (the dielectric constant: 7.426) solvent has been used in this work with the model of Polarizable Continuum Model (PCM) using the integral equation formalism variant (IEFPCM) [40-42], which considers the solute in the cavity of overlapping solvent that own apparent charges to reproduce the electrostatic potential because of the polarized dielectric within the cavity. PCM models mitigate the computational burden of explicitly modeling solvent molecules and the specific interactions with the solute. The solvent is treated as a constant dielectric reaction field where the charge density of the solute is projected onto a grid on the surface of a solvent cavity and polarized based on the value of the solvent dielectric. The resulting polarized charges on the cavity affect the charge density of the molecule and so on until self-consistency is achieved.

The S_0-state geometries were optimized without constraint for all the species in this work. And the vibrational frequencies have been analyzed at the optimized structures to verify that all these forms correspond to the local minima on the S_0-state potential energy surface. Harmonic vibrational frequencies with normal mode force constants, anharmonic vibrational frequencies with normal mode force constants, dipole moments, and dipole moment first derivatives were calculated for all solvent phase optimized structures. In view of the vertical excitation energy calculations, they can be carried out from the S_0-state optimized structure using TDDFT method with default solvation (i.e., linear reaponse and non-equilibrium). And six low-lying excited states have been predicted in this work. The S_1-state geometries were optimized with constraint based on the ground-state optimized

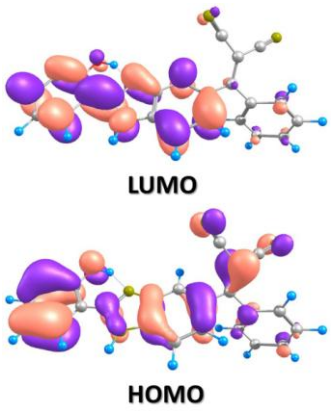

Figure 2: The theoretical frontier molecular orbitals (HOMO and LUMO) for HBPMM system.

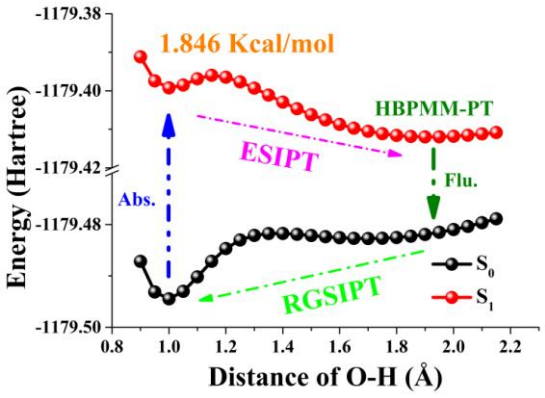

Figure 3: The constructed S_0-state and S_1-state potential energy curves for HBPMM molecule along with the proton-transfer reaction path. The potential energy barrier for the S_1-state proton transfer process is also shown in this figure.

geometries. And the vibrational frequencies were also analyzed to confirm their stabilities. Analyses of frequency can obtain the thermodynamic corrections in the corresponding electronic states. Zero-point energy correction and thermal corrections to the Gibbs free energy were also performed according to the harmonic vibrational frequencies.

The self-consistent field (SCF) convergence thresholds of the energy for both S_0 and S_1 states optimizations have been set to 10^{-8} (the default setting is 10^{-6}). Fine quadrature grids of size 4 are employed. The Harmonic vibrational frequencies in both S_0 and S_1 states are determined by diagonalization of the Hessian. The excited state Hessian is obtained by central differences and default displacement of 0.02 Bohr. The infrared intensities are determined from the gradients of dipole moment.

3. Results and discussion

As mentioned above, the S_0-state configuration of the sensor molecule HBPMM has been optimized using the B3LYP functional with the TZVP basis set. And to evaluate the solvent effect, tetrahydrofuran solvent has been also considered in this calculation according to the IEFPCM model. As shown in **Figure 1**, the S_0-state forms of HBPMM, its proton-transfer form HBPMM-PT, the fluoride complex structure HBPMM-F, and the anion form HBPMM-A are all optimized. Clearly, the intramolecular hydrogen bond O-H•••N exists in the HBPMM molecule. Since the photo-excitation process, the changes about intramolecular hydrogen bond may facilitates the ESIPT reaction along with O-H•••N, we firstly explore the primary structural parameters about bond lengths and bond angles involved in the hydrogen bond. The corresponding results have been listed in **Table 1**. It can be clearly found that the bond distance of O-H changes from S_0-state 0.994 Å to S_1-state 1.005 Å, while the H•••N bond lengths shortens from 1.722 Å to 1.682 Å. That is to say, the intramolecular hydrogen bond should be shortened in the S_1 state upon the photo-excitation process. Further, comparing the bond angle δ(O-H•••N) of HBPMM structure, we found bond angle is also increased from S_0-state 147.2º to S_1-state 148.6º. Coupling with the changed feature of bond distances, we confirm that the intramolecular hydrogen bond O-H•••N should be strengthening in the S_1 state [43-50]. Moreover, to the best of our knowledge, the simulated infrared (IR) vibrational spectra involved in hydrogen bonding moieties should be also another manner to explore excited state intramolecular hydrogen bonding dynamics [51-63]. Thus, we also calculated the IR vibrational spectra about the O-H stretching vibration. The results show that S_0-state O-H stretching vibration of HBPMM is located at 3182 cm^{-1}, which changes to be 2981 cm^{-1} in the S_1 state. In other words, the large red shift 201 cm^{-1} should be attributed to the strengthening intramolecular hydrogen bond O-H•••N upon the photo-excitation process. Thus we could confirm the hydrogen bond O-H•••N is enhanced in the first excited state, which provides the possibility for the ESIPT reaction.

In order to further check the effects resulting from photo-excitation process, we also investigate the variations about charge distribution for HBPMM form. The vertical excitation process has been calculated with considering the six low-lying transitions using TDDFT/B3LYP/TZVP theoretical level. The absorption peak of $S_0 \rightarrow S_1$ transition is calculated to be 355 nm, which is consistent with experimental result 370 nm [31]. And the normal fluorescence peak (389 nm) is also simulated from the optimized S_1-state HBPMM structure, which was not reported in previous experiment that may be due to the ultrafast ESIPT reaction. And in view of the S_1-state proton-transfer HBPMM-PT form, the emission peak is calculated to be 511 nm, which is in agreement with the novel fluorescence peak 505 nm reported in previous experiment [31]. Therefore, we can say that our theoretical level is suitable for HBPMM system in this work. In addition, since the frontier molecular orbitals (MOs) should be a well manner to analyze the photo-excitation process [51-63], the highest occupied molecular orbital (HOMO) and the lowest unoccupied molecular orbital (LUMO) have been shown in **Figure 2**. Herein, we only show these two orbitals due to the first transition ($S_0 \rightarrow S_1$) mainly involved in these two orbitals. The differences of charge distribution between HOMO and LUMO can be clearly seen in this figure, which indicates the first excited state should be

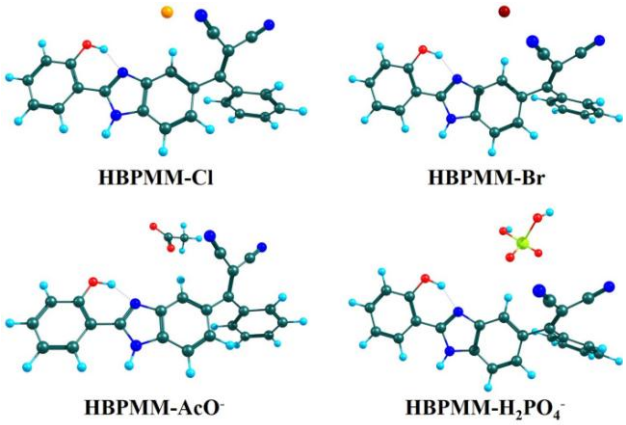

Figure 4: View of the corresponding structures of HBPMM-Cl, HBPM-Br, HBPMM-AcO^- and HBPM-$H_2PO_4^-$ complexes optimized based on DFT/B3LYP/TZVP/IEFPCM (tetrahydrofuran) theoretical level.

Table 1. The calculated primary bond lengths (Å) and angles (º) of HBPMM and HBPMM-PT forms in the S_0 and S_1 states based on the DFT and TDDFT methods in tetrahydrofuran solvent, respectively.

	HBPMM		HBPMM-PT	
	S_0	S_1	S_0	S_1
O-H	0.994	1.005	1.696	1.917
H-N	1.722	1.682	1.043	1.020
δ(O-H···N)	147.2º	148.6º	135.1º	126.6º

Table 2. The theoretical binding energies E (kcal/mol) for HBPMM chemosensor with anions (F-, Cl-, Br-, AcO- and H2PO4-) using the B3LYP/TZVP theoretical level in tetrahydrofuran solvent.

	F^-	Cl^-	Br^-	AcO^-	$H_2PO_4^-$
E	23.69	10.54	8.79	9.54	7.48

attributed to the intramolecular charge transfer (ICT) state. In view of the moieties around the hydrogen bond, it can be found the decrease of charge density of hydroxyl from HOMO to LUMO orbital, which means the increase of acidic property of hydroxyl. In other words, the hydrogen proton of hydroxyl of HBPMM changes to be much more active due to the photo-excitation process. Thus, the ESIPT reaction is supported due to the charge redistribution.

As far as we know, the theoretical constructed potential energy curves could provide reasonable explanations about the excited state dynamical processes [64-72]. Thus, in this work, we adopt this manner to explore the ESIPT behavior for HBPMM system. The constructed potential energy curves have been displayed in **Figure 3**, which have been performed based on fixing O-H bond length from 0.9 Å to 2.2 Å in step of 0.05 Å via DFT and TDDFT in both S_0 and S_1 states, respectively. In effect, we want to mention that the correct ordering of the closely spaced excited state might not be expected to become accurate to yield via TDDFT method, while previous theoretical work has indicates that this method could be reliable to provide qualitative energetic pathways for ESIPT calculations. As shown in **Figure 3**, the S_0-state potential energy increases along with the elongation of O-H bond distance, which means the forward proton transfer reaction cannot occur for HBPMM molecule. While when it comes to the S_1 state, it should be noted that there is a low potential energy barrier 1.846 kcal/mol for the proton transfer reaction. The low barrier indicates the ESIPT process should be ultrafast, which demonstrates the fluorescence of HBPMM itself is difficult to be detected experimentally. That should be the reason why only the emission (505 nm) of HBPMM-PT could be observed in experiment [31]. And our theoretical fluorescence peak of HBPM-PT form is 511 nm, which is close to experimental report. Till now, we have clarified the ESIPT mechanism for HBPMM system: Upon the photo-excitation, the S_0-state HBPMM can be excited to the S_1-state stable HBPMM form, which undergoes the ultrafast ESIPT process forming HBPMM-PT structure in the S_1 state. Then via radiation transition, the S_1-state HBPMM-PT emits fluorescence with forming S_0-state HBPMM-PT configuration that undergoes the reversed ground state intramolecular proton transfer reaction back to initial S_0-state HBPMM structure, which closes the four cycle reaction.

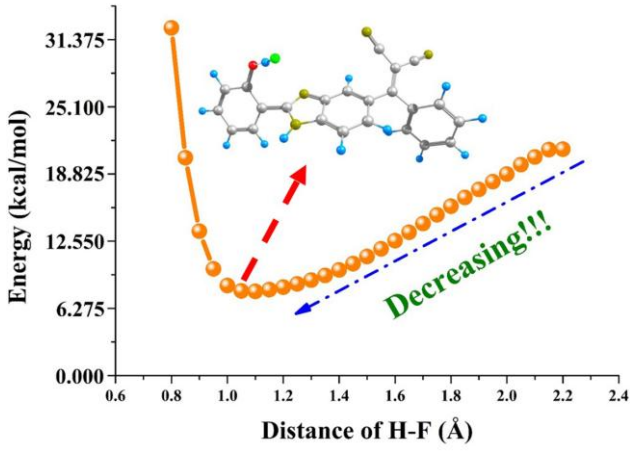

Figure 5: The potential energy curve of S_0 state for HBPMM chemosensor with the addition of fluoride anion. Herein, the functions of H-F distances in the S_0 state are from 2.20 Å to 0.80 Å in step of 0.05 Å.

Given the addition of fluoride anions, it can be found that the fluoride anions attack the hydroxyl moiety forming the HBPMM-F complex in the S_0 state as shown in **Figure 1**. One thing should be noticed that the fluoride anion-added deprotonation forming HBPMM-A structure via hydrogen bond could be adopted to interpret the response mechanism for fluoride ion probe. To compare with other anions mentioned in previous experiment, we also selected four common anions (Cl^-, Br-, AcO^- and $H_2PO_4^-$) and optimized the corresponding anion complexes to compare with HBPMM-F in this work. The corresponding chemical stable structures for these complexes are shown in **Figure 4**. The investigations about the binding energies between sensor itself and the anions should be reasonable for explaining the selectivity about anions [21-30]. As mentioned above, all the optimizations about all the complexes have been carried out via DFT/B3LYP/TZVP theoretical level in tetrahydrofuran solvent. And the calculations about binding energies are based on the formula: E (binding energy) = $E_{HBPMM} + E_{Anion} - E_{complex}$. Furthermore, in view of the intermolecular interactions, we also considered the basis set superposition error (BSSE) manner to make the binding energy accurate. The theoretical binding energies of the relative complexes have been listed in **Table 2**. Clearly, the binding energy between HBPMM and fluoride anion should be the biggest one (23.69 kcal/mol), which is much larger than the others. That is to say, the addition of fluoride anion should be the most received one to interact with HBPMM molecule in the ground state. Moreover, our simulated H-F bond lengths of HBPMM-F complex is about 1.006 Å, which is also close to the bond distance of HF molecule (0.92 Å) in the gas state [73].

Furthermore, to further explore the effects bringing from the fluoride-triggered deprotonation reaction in the fluoride-sensing mechanism for HBPMM system, we also simulated the relative S_0-state potential energy curve as shown in **Figure 5**. The constructed potential energy curve is based on shortening the distance of F atom and the H atom of hydroxyl for HBPMM molecule, which is selected from 2.20 Å to 0.80 Å with fixing the step of 0.05 Å. Similar with discussing the ESIPT mechanism about HBPMM above, the investigation about potential energy curve should be a good manner to deal with the protonated and deprotonated reactions in both ground and exited states [64-72]. It could be clearly found that the potential energy curve decreases along with the shortening of H and F atoms until the length of H-F reaching around 1.0 Å. In other words, the fluoride-triggered deprotonation reaction occurs spontaneously forming the HBPMM-A structure in the S_0 state. And given the steady-state electronic spectra, we also calculated the absorption peak and fluorescence peak of HBPMM-A form. The theoretical results are also close to experimental report. Thus till now, we explain the fluoride-sensing mechanism for HBPMM system that the deprotonation reaction bringing from fluoride anion inhibits the initial ESIPT process of HBPMM, which results in the novel changes of UV-Vis spectra that plays the roles in fluorescence response.

4. Conclusions

Summary up, in this present work, we theoretically explore the excited state hydrogen bonding dynamics, ESIPT mechanism and fluoride anion chemosensor for the novel HBPMM system. Via checking the formation of intramolecular hydrogen bond of HBPMM and verifying the strengthening excited state hydrogen bond, we present the possibility for the ESIPT process of HBPMM molecule. Further, given the photo-excitation process, we confirm that the charge redistribution around hydroxyl moiety of HBPMM provides the driving force for ESIPT reaction in the S_1 state. And theoretical insights into the potential energy curves, we clarify the ultrafast ESIPT process for HBPMM system. Then via exploring the fluoride-triggered fluorescence response, we find that the addition of fluoride anions could spontaneously capture the H proton of hydroxyl with forming intermolecular hydrogen bond O-H•••F. Due to the exothermal deprotonation process for HBPMM-F complex, the HBPMM-A configuration can be formed in the S_0 state. While for other anions, the corresponding deprotonation process is endothermic. This work not only presents the unambiguous sensing mechanism of fluoride anion, but also paves the way for synthesizing and designing fluorescent sensors in future.

Acknowledgements

This work was supported by the National Natural Science Foundation of China (grant no. 11604333) and the Taishan Scholars project of Shandong Province (ts201712011), the Innovative Talent Support Program of Liaoning Province (Grant No. LR2017062), the Liaoning Provincial Department of Education Project (Grant No. LFW201710).

References

[1] F. Yu, P. Song, P. Li, B. Wang, K. Han, Analyst **2012**, 137, 3740.
[2] J. Zhao, K. Xu, W. Yang, Z. Wang, F. Zhong, Chem. Soc. Rev. **2015**, 44, 8904.
[3] J. Zhao, W. Wu, J. Sun, S. Guo, Chem. Soc. Rev. **2013**, 42, 5323.
[4] F. B. Yu, P. Li, B. S. Wang, K. L. Han, J. Am. Chem. Soc. **2013**, 135, 7674.
[5] Z. Lou, P. Li, K. Han, Acc. Chem. Res. **2015**, 48, 1358.
[6] J. Shao, H. Sun, H. Guo, S. Ji, J. Zhao, W. Wu, X. Yuan, C. Zhang, T. James, Chem. Sci. **2012**, 3, 1049.
[7] G. Li, W. Li, H. Zhang, X. Sun, J. Theo. Comput. Chem. **2014**, 13, 1450006.
[8] G. Li, P. Song, G. He, Chin. J. Chem. Phys. **2011**, 24, 305.
[9] F. Yu, P. Li, P. Song, B. Wang, J. Zhao, K. Han, Chem. Commun. **2012**, 48, 2852.
[10] F. Yu, P. Li, G. Li, G. Zhao, T. Chu, K. Han, J. Am. Chem. Soc. **2011**, 133, 11030.
[11] A. Rostami, A. Colin, X. Li, M. Chudzinski, A. Lough, M. Taylor, J. Org. Chem. **2010**, 75, 3983.
[12] Q. Wang, Y. Xie, Y. Ding, X. Li, W. Zhu, Chem. Commun. **2010**, 46, 3669.
[13] X. Peng, Y. Wu, J. Fan, M. Tian, K. Han, J. Org. Chem. **2005**, 170, 10524.
[14] Y. Wu, X. Peng, J. Fan, S. Gao, M. Tian, J. Zhao, S. Sun, J. Org. Chem. **2007**, 72, 62.
[15] P. Singh, M. Barjatiya, S. Dhing, R. Bhatnagar, S. Kothari, V. Dhar, Urol. Res. **2001**, 29, 238.
[16] X. Cui, J. Zhao, Z. Lou, S. Li, H. Wu, K. Han, J. Org. Chem. **2015**, 80, 568.
[17] J. Zhao, J. Chen, Y. Cui, J. Wang, L. Xia, Y. Dai, P. Song, F. Ma, Phys. Chem. Chem. Phys. **2015**, 17, 1142.
[18] Z. Lou, S. Yang, P. Li, P. Zhou, K. Han, Phys. Chem. Chem. Phys. **2014**, 16, 3749.
[19] Y. Ma, L. Zhao, Y. Li, J. Liu, Y. Yang, T. Chu, Tetrahedron, **2018**, 74, 3584.
[20] J. Zhao, J. Chen, J. Liu, M. Hoffmann, Phys. Chem. Chem. Phys. **2015**, 17, 11990.
[21] G. Li, T. Chu, Phys. Chem. Chem. Phys. **2011**, 13, 20766.
[22] J. Chen, M. Yuan, J. Wang, Y. Yang, T. Chu, J. Phys. Chem. A **2014**, 118, 8986.
[23] T. Chu, B. Liu, Int. Rev. Phys. Chem. **2016**, 35, 187.
[24] G. Li, K. Han, WIREs Comput. Mol. Sci. **2018**, 8, e1351.
[25] J. Chen, P. Zhou, L. Zhao, T. Chu, RSC Adv. **2014**, 4, 254.
[26] G. Li, G. Zhao, K. Han, G. He, J. Comput. Chem. **2011**, 32, 668.
[27] J. Chen, R. Liu, Y. Yang, T. Chu, Theor. Chem. Acc. **2014**, 133, 1411.
[28] J. Xu, J. Chen, S. Dong, A. Fu, H. Li, T. Chu, J. Phys. Org. Chem. **2016**, 29, 305.
[29] G. Li, G. Zhao, Y. Liu, K. Han, G. He, J. Comput. Chem. **2010**, 31, 1759.
[30] J. Chen, F. Zhao, Y. Yang, T. Chu, RSC Adv. **2015**, 5, 36279.
[31] A. Gupta, A. Gary, K. Paul, V. Luxami, J. Lumin. **2016**, 173, 165.
[32] M. J. Frisch, G. W. Trucks, H. B. Schlegel, G. E. Scuseria, M. A. Robb, J. R. Cheeseman, G. Scalmani, V. Barone, B. Mennucci, G. A. Petersson, H. Nakatsuji, M. Caricato, X. Li, H. P. Hratchian, A. F. Izmaylov, J. Bloino, G. Zheng, J. L. Sonnenberg, M. Hada, M. Ehara, K. Toyota, R. Fukuda, J. Hasegawa, M. Ishida, T. Nakajima, Y. Honda, O. Kitao, H. Nakai, T. Vreven, J. A. Montgomery Jr, J. E. Peralta, F. Ogliaro, M. Bearpark, J. J. Heyd, E. Brothers, K. N. Kudin, V. N. Staroverov, T. Keith, R. Kobayashi, J. Normand, K. Raghavachari, A. Rendell, J. C. Burant, S. S. Iyengar, J. Tomasi, M. Cossi, N. Rega, J. M. Millam, M. Klene, J. E. Knox, J. B. Cross, V. Bakken, C. Adamo, J. Jaramillo, R. Gomperts, R. E. Stratmann, O. Yazyev, A. J. Austin, R. Cammi, C. Pomelli, J. W. Ochterski, R. L. Martin, K. Morokuma, V. G. Zakrzewski, G. A. Voth, P. Salvador, J. J. Dannenberg, S. Dapprich, A. D. Daniels, O. Farkas, J. B. Foresman, J. V. Ortiz, J. Cioslowski and D. J. Fox, Gaussian 09, revision D.01; Gaussian, Inc., Wallingford, CT, **2009**.
[33] C. Lee, W. Yang, R. Parr, Phys. Rev. B **1988**, 37, 785.
[34] B. Miehlich, A. Savin, H. Stroll, H. Preuss, Chem. Phys. Lett. **1989**, 157, 200.
[35] W. Kolth, A. Becke, R. Parr, J. Phys. Chem. **1996**, 100, 12974.
[36] S. Vosko, L. Wilk, M. Nusair, Can. J. Phys. **1980**, 58, 1200.
[37] O. Treutler, R. Ahlrichs, J. Chem. Phys. **1995**, 102, 346.
[38] F. Furche, R. Ahlrichs, J. Chem. Phys. **2002**, 117, 7433.
[39] D. Feller, J. Comput. Chem. **1996**, 17, 1571.
[40] R. Cammi, J. Tomasi, J. Comput. Chem. **1995**, 16, 1449.
[41] B. Mennucci, E. Cances, J. Tomasi, J. Phys. Chem. B **1997**, 101, 10506.
[42] E. Cances, B. Mennucci, J. Tomasi, J. Chem. Phys. **1997**, 107, 3032.
[43] G. Zhao, K. Han, Biophy. J. **2008**, 94, 38.
[44] G. Zhao, K. Han, J. Phys. Chem. A **2009**, 113, 4788.
[45] G. Zhao, B. Northrop, K. Han, P. Stang, J. Phys. Chem. A **2010**, 114, 9007.
[46] L. Zhou, J. Liu, G. Zhao, Y. Shi, X. Peng, K. Han, Chem. Phys. **2007**, 333, 179.
[47] G. Zhao, K. Han, Acc. Chem. Res. **2012**, 45, 404.
[48] G. Zhao, K. Han, J. Comput. Chem. **2008**, 29, 2010.
[49] C. Miao, Y. Shi, J. Comput. Chem. **2011**, 32, 3058.
[50] G. Zhao, K. Han, J. Chem. Phys. **2007**, 127, 024306.
[51] Y. Liu, S. Lan, C. Zhu, S. Lin, J. Phys. Chem. A **2015**, 119, 6269.
[52] Y. Liu, S. Wang, C. Wang, C. Zhu, K. Han, S. Lin, J. Chem. Phys. **2016**, 145, 164314.

[53] X. Liu, H. Yin, H. Li, Y. Shi, Spectrochimica Acta Part A **2017**, 177, 1.
[54] Y. Liu, S. Lan, C. Li, Spectrochimica Acta Part A **2013**, 112, 257.
[55] H. Li, J. Han, H. Zhao, X. Liu, L. Ma, C. Sun, H. Yin, Y. Shi, J. Clust. Sci. **2018**, 29, 585.
[56] H. Yin, H. Li, G. Xia, C. Ruan, Y. Shi, H. Wang, M. Jin, D. Ding, Sci. Rep. **2016**, 6, 19774.
[57] S. Lan, Y. Liu, Spectrochimica Acta Part A **2015**, 139, 49.
[58] Y. Cui, H. Zhao, J. Zhao, P. Li, P. Song, L. Xia, New J. Chem. **2015**, 39, 9910.
[59] H. Li, Y. Shi, H. Yin, Y. Wang, L. Cong, M. Jin, D. Ding, Spectrochimica Acta Part A **2015**, 141, 211.
[60] Q. Wei, Q. Zhou, M. Zhao, M. Zhang, P. Song, J. Lumin. **2017**, 183, 7.
[61] H. Li, H. Yin, X. Liu, Y. Shi, M. Jin, D. Ding, Spectrochimica Acta Part A **2017**, 184, 270.
[62] J. Zhao, Y. Zheng, Sci. Rep. **2017**, 7, 44897.
[63] H. Liu, M. Mehata, S. Lan, Spectrochimica Acta Part A **2014**, 128, 280.
[64] Y. Cui, H. Zhao, L. Jiang, P. Li, Y. Ding, P. Song, L. Xia, Comput. Theor. Chem. **2015**, 1074, 125.
[65] M. Zhang, Q. Zhou, M. Zhang, Y. Dai, P. Song, Y. Jiang, J. Clust. Sci. **2017**, 28, 1191.
[66] Y. Dai, M. Zhang, M. Zhang, L. Sun, J. Meng, P. Song, Spectrochimica Acta Part A **2018**, 200, 345.
[67] M. Zhang, Q. Zhou, C. Du, Y. Ding, P. Song, RSC Adv. **2016**, 6, 59389.
[68] Y. Liu, S. Wang, C. Zhu, S. Lin, New J. Chem. **2017**, 41, 8437.
[69] Q. Wei, J. Wang, M. Zhao, M. Zhang, Y. Song, P. Song, Can. J. Chem. **2018**, 96, 83
[70] Y. Cui, Y. Li, Y. Dai, F. Verpoort, P. Song, L. Xia, Spectrochimica Acta Part A **2016**, 154, 130.
[71] H. Yin, Y. Shi, Y. Wang, Spectrochimica Acta Part A **2014**, 129, 280.
[72] A. Sobolewski, W. Domcke, Phys. Chem. Chem. Phys. **1999**, 1, 3065.
[73] D. Lide, CRC handbook of chemistry and physics, 84th ed, CRC Press, Cleveland, **2004**.